Available online at www.sciencedirect.com
SCIENCE DIRECT®
Proceedings of the Combustion Institute 30 (2005) 1775–1782
Proceedings of the Combustion Institute
www.elsevier.com/locate/proci

Effect of swirl on combustion dynamics in a lean-premixed swirl-stabilized combustor

Ying Huang*, Vigor Yang

The Pennsylvania State University, University Park, PA 16802, USA

Abstract

The effect of inlet swirl on the flow development and combustion dynamics in a lean-premixed swirl-stabilized combustor has been numerically investigated using a large-eddy-simulation (LES) technique along with a level-set flamelet library approach. Results indicate that when the inlet swirl number exceeds a critical value, a vortex-breakdown-induced central toroidal recirculation zone is established in the downstream region. As the swirl number increases further, the recirculation zone moves upstream and merges with the wake recirculation zone behind the centerbody. Excessive swirl may cause the central recirculating flow to penetrate into the inlet annulus and lead to the occurrence of flame flashback. A higher swirl number tends to increase the turbulence intensity, and consequently the flame speed. As a result, the flame surface area is reduced. The net heat release, however, remains almost unchanged because of the enhanced flame speed. Transverse acoustic oscillations often prevail under the effects of strong swirling flows, whereas longitudinal modes dominate the wave motions in cases with weak swirl. The ensuing effect on the flow/flame interactions in the chamber is substantial.

Keywords: Combustion instabilities; Premixed; Swirl; Large-eddy simulation; Level-set

1. Introduction

Combustion instabilities are commonly encountered in the development of lean-premixed (LPM) gas-turbine engines [1–4]. The spontaneous generation of unsteady flow oscillations in the combustion chamber may cause structural vibration and excessive heat transfer to the chamber, and consequently lead to failure of the system. Most LPM gas-turbine engines utilize swirling flows to stabilize the flame for efficient and clean combustion. One of the most important flow features produced by a swirl injector is a central toroidal recirculation zone (CTRZ), which serves as a flame stabilization mechanism. Flows in this region are, in general, associated with high shear rates and strong turbulence intensities resulting from vortex breakdown. Although this type of flows has been extensively studied, there remain many unresolved issues, such as swirl generation, vortex breakdown, axisymmetry breaking, and azimuthal instability [5–7]. In particular, the effect of flow swirl on combustion dynamics has not been well studied, at least in a quantitative sense. Swirling flows may affect flame dynamics in two aspects. First, large-scale unsteady motions arising from shear-layer instability and vortex breakdown, as well as precession of vortex core (PVC), may couple resonantly with acoustic waves in the combustor,

* Corresponding author. Fax: +1 814 865 3389.
E-mail address: huangying@psu.edu (Y. Huang).

1540-7489/$ - see front matter © 2004 Published by Elsevier Inc. on behalf of The Combustion Institute.
doi:10.1016/j.proci.2004.08.237

and subsequently cause combustion instabilities. Second, flow swirl may alter the flame structure and combustion intensity, and as a consequence influence the heat-release behavior in a combustion chamber. The ensuing effects on the stability characteristics could be substantial.

Several attempts have been conducted to investigate the effect of swirl on the flow and flame dynamics in combustion systems. Tangirala et al. [8] studied the influence of swirl and heat release on the flow structures and flame properties in a non-premixed swirl burner. Their results showed that mixing and flame stability can be improved by increasing the swirl number up to approximately unity, beyond which further increase in swirl actually reduced the turbulence level and flame stability. Broda et al. [9] and Seo [10] performed an experimental study of combustion dynamics in a lean-premixed swirl-stabilized combustor. The dominant acoustic motion corresponds to the first longitudinal mode of the chamber. An increase in swirl number tends to decrease the instability amplitude. Numerical simulations based on large-eddy-simulation (LES) techniques have also been performed. Stone and Menon [11,12] investigated a swirl-stabilized combustor flow. The impact of varying swirl and equivalence ratio on flame dynamics was studied. Grinstein et al. [13] simulated the flow dynamics in a swirl combustor with either a single swirler or triple swirlers. Emphasis was placed on the effect of inlet conditions (including swirl number, inlet length, and characteristic velocity) on the unsteady flow dynamics in the combustors. Wang et al. [14] recently examined the vortical flow dynamics in a swirl injector with radial entry. Various flow instability mechanisms, such as the Kelvin–Helmholtz, helical, and centrifugal instabilities, as well as their mutual interactions, were investigated in detail.

Although much useful information has been obtained from the preceding studies, the effects of flow swirl on turbulent flame dynamics and the way it modifies the flow/flame interactions require further investigation. The purpose of the present work was to explore the influence of swirl on the combustion dynamics in a lean-premixed swirl-stabilized combustor using an LES technique, simulating the experimental conditions reported in [9,10]. In our previous work [1,2], we have investigated stable flame evolution, the flame bifurcation phenomenon, and unstable flame dynamics for a fixed inlet swirl number but with different inlet flow conditions. In this paper, the flow and flame dynamics under various swirl intensities will be addressed. The specific objectives were to: (1) study the effect of swirl on flow development, acoustic properties, and flame evolution; and (2) investigate the interactions between turbulent flame dynamics and flow oscillations.

2. Theoretical formulation and numerical method

The basis of the analysis is the LES technique previously developed for investigating LPM combustion instabilities in swirl-stabilized combustors [1,2]. The formulation employs the Favre-filtered conservation equations of mass, momentum, and energy in three dimensions. The subgrid-scale (SGS) terms are modeled using a compressible-flow version of the Smagorinsky model suggested by Erlebacher et al. [15]. The damping function of Van-Driest is used to account for the flow inhomogeneities near the walls. A level-set flamelet library approach, which has been successfully applied to simulate premixed turbulent combustion [1,2,16], is used here. In this approach, the filtered flame surface evolution is modeled using a level-set G-equation, where G is defined as a distance function outside the flame front. Thermophysical properties are obtained using a presumed probability density function (PDF) along with a laminar flamelet library. The model, as currently implemented, does not explicitly consider the flame stretch effect, which may alter the local flame structure and cause flame extinction. These effects need to be eventually included and will be explored in subsequent work.

Boundary conditions must be specified to complete the formulation. At the inlet boundary, the mass flow rate and temperature are specified. The pressure is obtained from a one-dimensional approximation to the axial momentum equation, i.e., $\partial p/\partial x = -\rho\partial u/\partial t - \rho u\partial u/\partial x$. The mean axial-velocity distribution follows the one-seventh power law by assuming a fully developed turbulent pipe flow. The radial and azimuthal velocities are determined from the swirler vane angle. Turbulence properties at the inlet are specified by superimposing broad-band disturbances with an intensity of 15% of the mean quantity onto the mean velocity profiles. In addition, the acoustic response to disturbances arising downstream is modeled by means of an impedance function [1,16]. At the outlet boundary, the characteristic conditions proposed by Poinsot and Lele [17] are applied, and a time-invariant back pressure is specified as obtained from a simplified one-dimensional momentum equation $\partial p/\partial r = \rho U_\theta^2/r$ in the radial direction, where U_θ is the mean azimuthal velocity. The pressure at $r = 0$ is fixed as a pre-specified value. Finally, the no-slip adiabatic conditions are enforced along all the solid walls.

The resultant governing equations and boundary conditions are numerically solved by means of a density-based, finite-volume methodology. The spatial discretization employs a second-order, central-differencing method in generalized coordinates. Fourth-order matrix dissipation along with a total-variation-diminishing switch developed by Swanson and Turkel [18], and tested by Oefelein and Yang [19] is included to ensure

computational stability and to prevent numerical oscillations in regions with steep gradients. Temporal discretization is obtained using a four-step Runge–Kutta integration scheme. A multi-block domain decomposition technique along with static load balance is used to facilitate the implementation of parallel computation, with a message-passing interface at the domain boundaries. The theoretical and numerical framework described above has been validated by Huang et al. [1,16], and Apte and Yang [20] against a wide variety of flow problems to establish its credibility and accuracy.

3. Physical model and grid resolution

The physical model considered here consists of a single swirler injector, an axi-symmetric chamber, and a chocked nozzle, simulating the experimental setup described in [9,10]. Natural gas is injected radially from the center body through ten holes immediately downstream of the swirler vanes. The fuel/air mixture is assumed to be perfectly premixed before entering the combustor. The chamber measures 45 mm in diameter and 235 mm in length. The baseline condition includes an equivalence ratio of 0.573 and a chamber pressure of 0.463 MPa. The mass flow rates of the natural gas and air are 1.71 and 50.70 g/s, respectively. The inlet flow velocity of 86.6 m/s gives rise to a Reynolds number of 35,000 based on the height of the inlet annulus. The inlet temperature of 660 K corresponds to the case of unstable combustion reported in [9,10]. Two different swirl angles of 30° and 55° are investigated in the current study. The corresponding swirl numbers, defined as the ratio of the axial flux of the tangential momentum to the product of the axial momentum flux and a characteristic radius, are 0.44 and 1.10, respectively.

According to the experimental observations, the dominant acoustic motion in the axial direction corresponds to the first longitudinal mode. Since there exists an acoustic pressure node at the middle of the chamber, the computational domain includes both a portion of the inlet annulus downstream of the swirler vane and the upstream half of the chamber with a time-invariant back pressure specified at the exit plane. To avoid the numerical singularity along the combustor centerline, a central-square grid system (which consists of a square grid near the centerline and a cylindrical grid in the outer region) is adopted. The entire grid system has 3.44 million points, which are clustered in the shear layers downstream of the dump plane and near the solid walls to resolve the steep flow gradients in these regions. The largest grid size (around 0.7 mm) falls in the inertial sub-range of the turbulent kinetic energy spectrum based on the inlet Reynolds number. The computational domain is divided into 72 blocks. All the calculations are conducted on a distributed-memory parallel computer with each block calculated on a single processor.

4. Results and discussion

4.1. Flow evolution

For each swirl number, calculations were performed for about four flow-through times (around 12 ms) after the flowfield had reached its stationary state to obtain statistically meaningful data for analyzing the flow dynamics. Figure 1 shows the streamline patterns and mean temperature fields on the x–r plane. Three distinct recirculation zones are observed in the low-swirl number case with $S = 0.44$, including a separation wake recirculation zone (WRZ) behind the centerbody, a corner recirculation zone (CRZ) due to the sudden enlargement of the combustor configuration, and a central toroidal recirculation zone (CTRZ) resulting from vortex breakdown. The wake recirculation zone, however, disappears at the high swirl number of $S = 1.10$. The overall flow development with respect to the inlet swirl number can be described as follows. If there is no swirl, only the wake and corner reciruclation zones exist. As the swirl number increases and exceeds a critical value, vortex breakdown takes place and leads to the formation of a central recirculation zone. As the swirl number increases further, the central recirculation zone moves upstream and merges with the wake recirculation zone. Consequently, the corner reciruclation zone becomes diminished. Similar results were reported by Chao [21] in his experimental study of the recirculation structure in a co-annular swirl combustor. The mean temperature fields clearly exhibit enveloped flames anchored at the rim of the centerbody and the corner of the backward-facing step. The flame is much more compact for the high swirl number case with $S = 1.10$, which is due to the enhanced flame speed resulting from the increased turbulence intensity, as we will show later.

Figure 2 shows the radial distributions of the mean velocity components and turbulent kinetic energy at various axial locations, where $r = 0$ corresponds to the centerline of the chamber. The negative axial velocities in the central and corner regions indicate the existence of recirculation zones. The incoming flows from the inlet annulus spread outward from the chamber centerline under the effect of the centrifugal force, producing positive radial velocities in the main flow passage. The stronger the swirl strength is, the faster the main flow moves toward the wall. As a result, the size of the corner recirculation zone is considerably reduced at the high swirl number of $S = 1.10$. The mean azimuthal velocity fields sug-

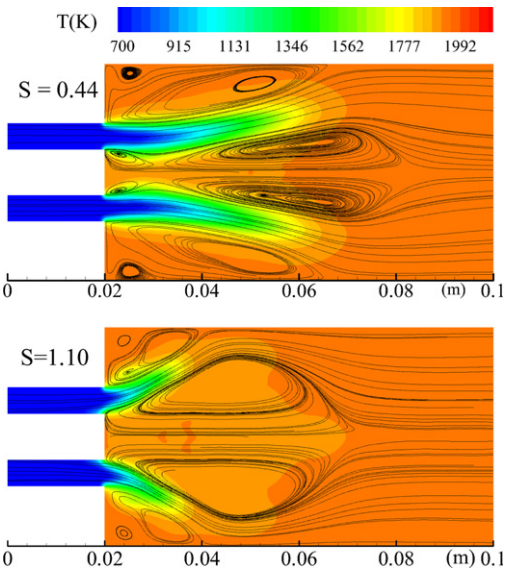

Fig. 1. Mean temperature fields and streamline patterns for two different swirl numbers.

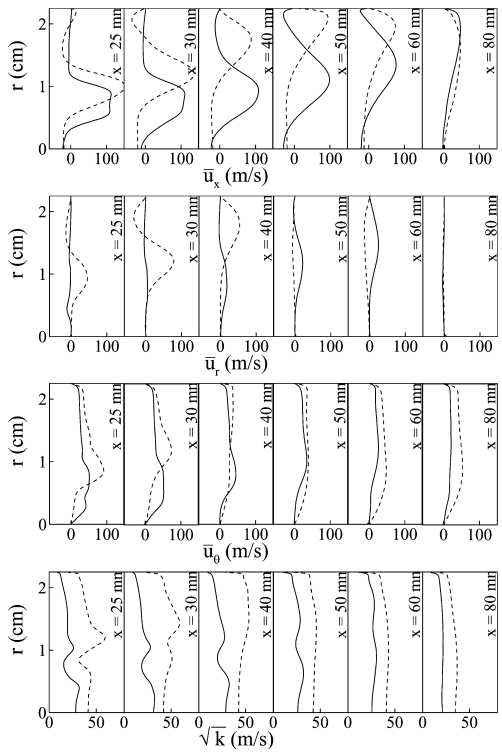

Fig. 2. Radial distributions of mean velocity components and turbulent kinetic energy at various axial locations for two different swirl numbers.

gest that the flow motion in the central region bears a close resemblance to solid-body rotation. The distributions of the turbulent kinetic energy indicate that a high turbulence-intensity region develops downstream of the centerbody and the backward-facing step, where large velocity fluctuations are produced because of the strong turbulent mixing in the shear layers between the incoming flow and the recirculation flows. The evolution of turbulent kinetic energy is governed by the following equation:

$$\mathrm{D}(\overline{u_i^2}/2)/\mathrm{D}t = \partial(-\overline{u_j p}/\rho_0 - \overline{u_i^2 u_j}/2 + 2\overline{\nu u_i e_{ij}})/\partial x_j - \overline{u_i u_j}\partial U_i/\partial x_j - 2\overline{\nu e_{ij} e_{ij}},$$

where $e_{ij} = (\partial u_i/\partial x_j + \partial u_j/\partial x_i)/2$. The existence of the steep velocity gradient $\partial U_i/\partial x_j$ due to the strong swirling and reverse flow at the high swirl number case facilitates the high production of turbulent kinetic energy, $-\overline{u_i u_j}\partial U_i/\partial x_j$. Consequently, a much stronger turbulent kinetic energy is observed for the high swirl number case with $S = 1.10$.

Figure 3 shows snapshots of the vorticity magnitude field on an x–r plane. For the low swirl number case with $S = 0.44$, large vortical structures, arising from the shear layers downstream of the dump plane and centerbody, are convected downstream, and then dissipated into small-scale eddies. The same phenomenon is also observed for the high swirl number case, in which well-organized vortices are shed from the edge of the backward-facing step. The vortex motions downstream of the centerbody, however, become quite

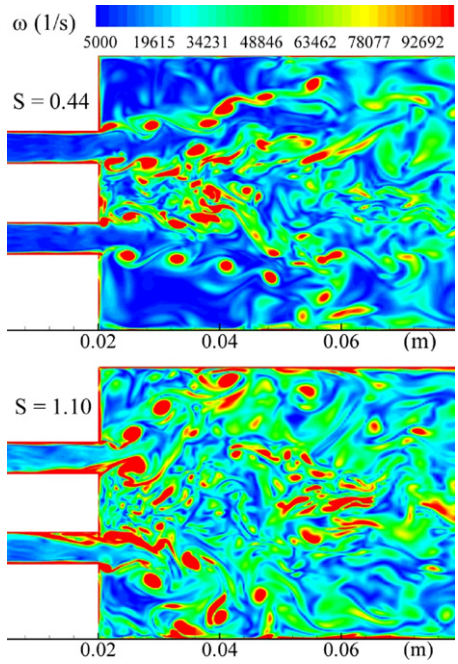

Fig. 3. Snapshots of vorticity magnitude field on an x–r plane for two different swirl numbers.

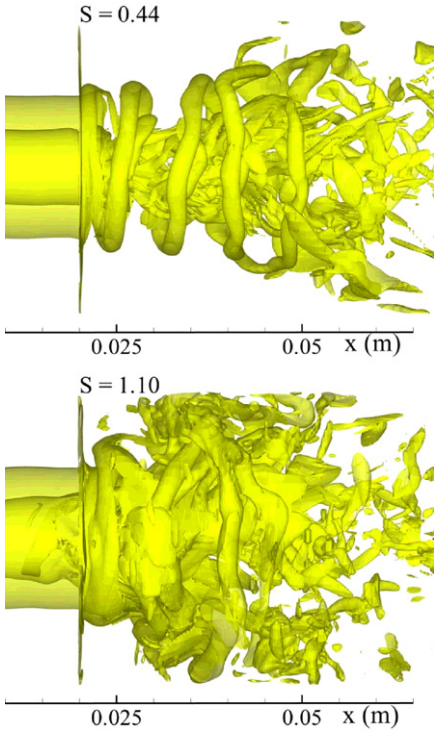

Fig. 4. Snapshots of iso-vorticity surface at $\omega = 75{,}000\ s^{-1}$ ($r > 0.02$ m is blanked) for two different swirl numbers.

disordered due to the presence of the strong central recirculating flow. In both cases, the vortex shedding frequencies are close to that of the first tangential mode of acoustic wave in the chamber.

Figure 4 shows snapshots of the iso-vorticity surface at $\omega = 75{,}000\ s^{-1}$. The flowfield in the region $r > 2$ cm is blanked to provide a clear picture of the vortex structures. For the low swirl number case with $S = 0.44$, a vortex spiral evolves from the shear layer originating at the backward-facing step due to the Kelvin–Helmholtz instabilities in both the axial and azimuthal directions. This vortical structure gyrates around the centerline and persists for about several turns before breaking up into small fragments. For the high swirl-number case with $S = 1.10$, a spiral vortex structure can also be observed. The structure, however, is much more complex, due to the high centrifugal force. It spreads outward rapidly and soon breaks up into small-scale structures.

4.2. Combustion dynamics

The oscillatory flowfield was carefully surveyed to provide direct insight into the driving mechanism for acoustic oscillations. A vast number of probes were employed to register the flow motions in various parts of the chamber. Figure 5 shows

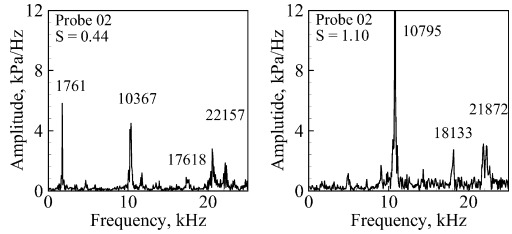

Fig. 5. Power spectral densities of pressure fluctuations immediately downstream of the dump plane for two different swirl numbers.

the frequency contents of the pressure fluctuations immediately downstream of dump plane. For $S = 0.44$, the dominant frequencies of 1761, 10,367, and 17,618 Hz correspond to first longitudinal (1L), first tangential (1T), and second tangential (2T) modes of acoustic motions in the chamber, respectively. For $S = 1.10$, the longitudinal wave disappears, and the frequencies of the 1T and 2T modes shift slightly to 10,795 and 18,133 Hz due to the change in the temperature field. The inlet swirl number exerts little influence on the acoustic frequencies but plays a significant role in determining the wave amplitudes. The suppression of low-frequency oscillations for the high swirl number case may be attributed to the enhanced flame stiffness, which reduces flame sensitivity to imposed disturbances.

To understand the mutual coupling between flame dynamics and flow oscillations, the total heat release and flame surface area were analyzed in the frequency domain. The overall heat release in the chamber can be obtained from:

$$\dot{Q} = \rho_u \Delta h_f^0 S_T A,$$

where ρ_u is the unburned gas density, S_T is the subgrid turbulent flame speed, Δh_f^0 is the heat of reaction, and A is the total filtered flame surface area. The total filtered flame surface area can be obtained from the following integral:

$$A = \int \delta(\tilde{G}(\mathbf{x}))|\nabla \tilde{G}(\mathbf{x})|\,d\mathbf{x},$$

where δ is a delta function, which needs to be numerically evaluated. In the level-set flamelet library approach [1,16], $\tilde{G}$ represents a signed distance function with $|\nabla \tilde{G}| = 1$, and $\tilde{G} = 0$ corresponds to the filtered flame front. $\delta(\tilde{G}) = 0$ almost everywhere except on the lower dimensional interface (i.e., flame surface). For the sake of simplicity without significant reduction in accuracy, a first-order accurate smeared out approximation of the delta function is usually used [22,23]:

$$\delta(\tilde{G}) = \begin{cases} [1 + \cos(\pi \tilde{G}/\varepsilon)]/2\varepsilon, & |\tilde{G}| < \varepsilon, \\ 0, & |\tilde{G}| > \varepsilon, \end{cases}$$

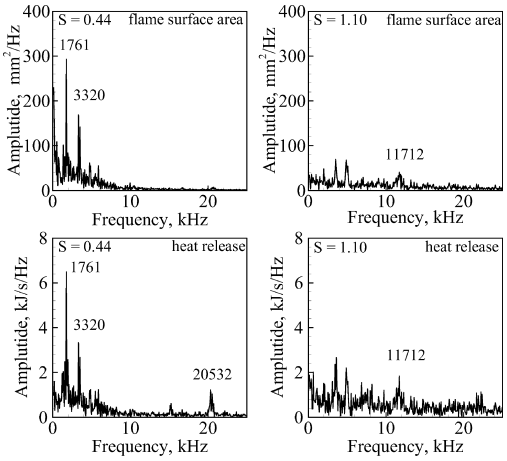

Fig. 6. Power spectral densities of total flame surface-area and heat-release fluctuations for two different swirl numbers.

where ε is a tunable parameter that determines the size of the bandwidth of numerical smearing. A typically value is $\varepsilon = 1.5\Delta$, with Δ being the grid width. This method has been widely used to evaluate the quantities defined on arbitrary interfaces in the areas of multi-phase flows, computer vision, and image processing [22,23].

Figure 6 shows the power spectral densities of the total filtered flame surface-area and heat-release fluctuations. At $S = 0.44$, there is a dominant mode at 1761 Hz in flame surface oscillation, which corresponds to the 1L acoustic mode of the combustor. A higher harmonic mode is also found at 3320 Hz, approximately twice the frequency of 1L mode. Although transverse acoustic motions including the 1T and 2T modes are observed, the flame surface-area oscillations do not exhibit such a high-frequency behavior. At $S = 1.10$, a small peak (11,712 Hz) near the 1T acoustic mode

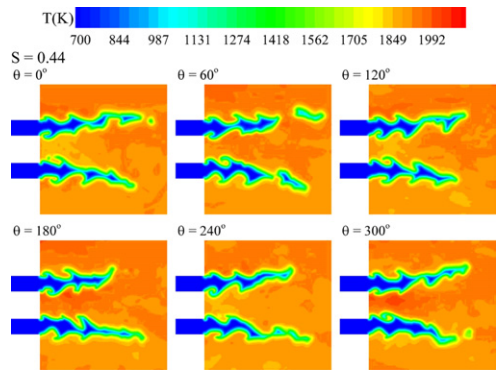

Fig. 7. Temporal evolution of temperature field on an x–r plane over one cycle of 1L mode of oscillation for $S = 0.44$.

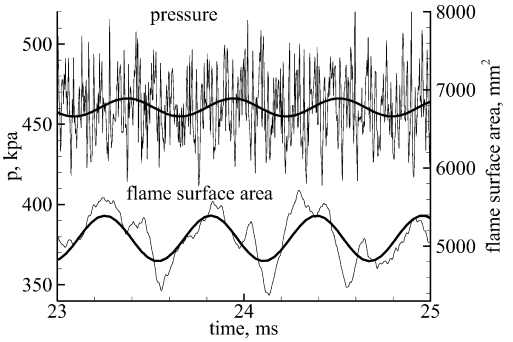

Fig. 8. Time histories of pressure immediately downstream of the dump plane (top) and flame surface-area (bottom) for $S = 0.44$. Thick black lines represent the extracted 1L oscillations.

is observed, but no corresponding 1L mode oscillation is found. The behavior of the total heat-release fluctuations in the frequency domain bears a close resemblance to that of flame surface-area variations, as shown in Fig. 6. However, a small spike near the frequency of 20,532 Hz is observed for $S = 0.44$, which arises from the fluctuations in the subgrid turbulent flame speed S_T [1,16]. In light of the above observations, one can conclude that low-frequency acoustic perturbations exert a

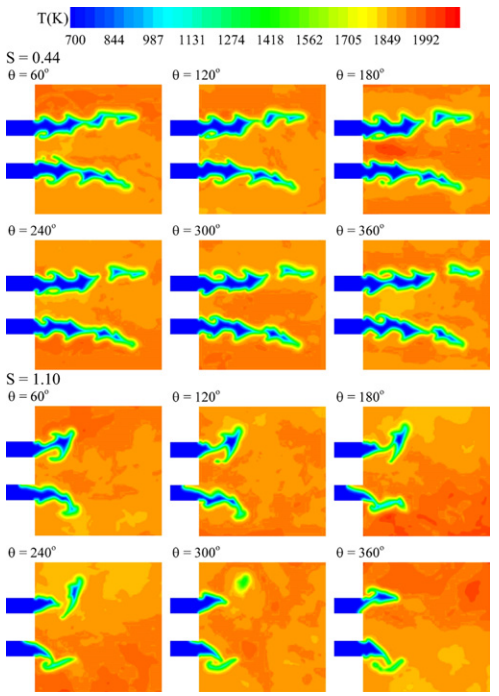

Fig. 9. Temporal evolution of temperature field on an x–r plane over one cycle of 1T mode of oscillation for two different swirl numbers.

strong influence on the fluctuations of the total flame surface-area and heat release. In contrast, high-frequency acoustic oscillations travel through the flame zone without significantly affecting the flame surface-area and heat-release variations. The results agree qualitatively well with the predictions from a companion analytical analysis of flame response reported in [16]. The calculated mean flame surface area and the root mean square value of fluctuation for the high swirl-number case are much smaller than those of the low swirl-number case. However, due to the increased turbulence intensity and the resultant enhancement of the flame speed for the high swirl-number case, the mean heat-release rate and the associated root mean square value of the fluctuating quantity are very close in these two cases.

Figure 7 presents the temporal evolution of the temperature field in the upstream section of the chamber on an x–r plane over one cycle of the 1L mode of acoustic oscillation at $S = 0.44$. The phase angle θ is referenced to the acoustic pressure of the 1L mode at the chamber head-end. The entire process is dictated by the entrainment and mixing of the cold flow with hot gases in the vortical structures in the flame zone. Flames are contorted and convoluted by these vortex structures, as observed in Fig. 4, thus revealing the interactions between the local flow evolution and flame dynamics.

Figure 8 shows the time histories of pressure immediately downstream of the dump plane (top) and the total flame surface area (bottom) for the lower swirl number case with $S = 0.44$. These signals involve a wide range of frequencies corresponding to turbulent fluctuations and acoustic oscillations. The extracted 1L oscillations (denoted by the thick black lines) of the pressure and flame surface area are also plotted for clarity. The flame surface-area variation can be elucidated by considering its interaction with the local oscillatory flowfield. It lags behind the pressure oscillation by 76°. During the period from $\theta = -166°$ ($t = 24.09$ ms) to 14° ($t = 24.38$ ms), a relatively lower pressure field exists near the dump plane. This facilitates the delivery of the fresh reactants into the chamber. Intensive heat release then occurs after a short fluid mixing and chemical induction time. The resultant flow expansion tends to push the flame outward and cause the flame surface area to increase from a trough to a crest. Unburned mixture fragments may break up away from the main stream and generate local hot spots when convected downstream. During the period of $\theta = 14°$ ($t = 24.38$ ms) to 194° ($t = 24.66$ ms), the relatively higher pressure field near the dump plane prevents the fresh reactants from traveling downstream into the chamber. The flame zone is thus reduced and becomes a little more compact. The process then repeats.

Figure 9 presents the temporal evolution of the temperature field in the upstream section of the chamber on the x–r plane over one cycle of the 1T mode of acoustic oscillation. For both swirl numbers, new vortices are produced at the edge of the backward-facing step and bulge the flame front. They continue to distort the flame or even produce separated flame pockets when traveling downstream, although for the high swirl number case this process is less apparent due to the reduced flame length. This kind of flame/vortex interaction is also observed downstream of the centerbody for the low swirl number case. As the swirl number increases, the flame anchored by the center recirculating flow may propagate upstream periodically and lead to flame flashback. Two mechanisms have been identified for the occurrence of flame flashback [2]. The first involves flame propagation in the boundary layer along a solid wall where the local velocity diminishes toward the surface. The second is associated with flow reversal, which is usually caused by vortical motions or acoustic oscillations. In the current case, the flashback is closely linked to the strong reverse flow in the center recirculation zone. The swirl strength is so strong that sometimes it causes the center recirculating flow to enter into the inlet annulus. As a result, the flame attached to the centerbody travels upstream and flashback occurs.

5. Conclusions

The effect of swirl on unsteady flame dynamics in a lean-premixed, swirl-stabilized combustor under unstable operating conditions has been numerically investigated in depth. Turbulence closure is achieved by means of a large-eddy-simulation technique along with a level-set flamelet library approach. The computed flow pattern and acoustic properties agree well with those experimentally observed, although no velocity field measurements are available for comparison purposes. The swirl strength has enormous effects on the flow development and flame dynamics in the combustion chamber. When the inlet swirl-number increases, the central recirculation zone due to the vortex breakdown moves upstream and eventually overrides the wake recirculation zone. A higher swirl number tends to increase the turbulence intensity and the flame speed, and consequently shorten the flame length. However, excessive swirl often causes the central recirculating flow to enter into the inlet annulus and leads to the occurrence of flame flashback. The inlet swirl number exerts little influence on the frequencies of the acoustic oscillations, but plays a dominant role in determining the amplitudes of wave motions. Another important observation is that low-frequency flow oscillations significantly affect the global behavior of the flame,

including total surface area and heat-release rate. In contrast, high-frequency flow motions have only a limited effect on flame oscillation, although they may impose a significant impact on the local flame properties. Results of this kind provide valuable information about flow/flame interactions in lean-premixed combustors with swirling flows.

Acknowledgment

The research work reported in this paper was sponsored by the Air Force Office of Scientific Research, Grant No. F49620-99-1-0290.

References

[1] Y. Huang, H.G. Sung, S.Y. Hsieh, V. Yang, *J. Propul. Power* 19 (2003) 782–794.
[2] Y. Huang, V. Yang, *Combust. Flame* 136 (2004) 383–389.
[3] T. Lieuwen, K. Mcmanus, *J. Propul. Power* 19 (2003) 721.
[4] H.C. Mongia, T.J. Held, G.C. Hsiao, R.P. Pandalai, *J. Propul. Power* 19 (2003) 822–829.
[5] A.K. Gupta, D.G. Lilley, N. Syred, *Swirl Flows. Abacus*, London, 1984.
[6] V. Sthern, F. Hussain, *Annu. Rev. Fluid Mech.* 31 (1999) 537–566.
[7] O.C. Paschereit, E. Gutmark, W. Weisenstein, *AIAA J.* 38 (2000) 1025–1034.
[8] V. Tangirala, R.H. Chen, J.F. Driscoll, *Combust. Sci. Technol.* 51 (1987) 75–95.
[9] J.C. Broda, S. Seo, R.J. Santoro, G. Shirhattikar, V. Yang, *Proc. Combust. Inst.* 27 (1998) 1849–1856.
[10] S. Seo, Ph.D. thesis, Department of Mechanical Engineering, The Pennsylvania State University, University Park, PA, 1999.
[11] C. Stone, S. Menon, *Proc. Combust. Inst.* 29 (2002) 155–160.
[12] C. Stone, S. Menon, *J. Turb.* 4 (2003) 020.
[13] F.F. Grinstein, T.R. Young, E.J. Gutmark, G. Li, G. Hsiao, H.C. Mongia, *J. Turb.* 3 (2002) 030.
[14] S.W. Wang, S.Y. Hsieh, V. Yang, in: *Proceedings of the 3rd Int. Symp. Turb. Shear Flow Phenom*, 2003, pp. 905–910.
[15] G. Erlebacher, M.Y. Hussaini, C.G. Speziale, T.A. Zang, *J. Fluid Mech.* 238 (1992) 155–158.
[16] Y. Huang, Ph.D. thesis, Department of Mechanical Engineering, The Pennsylvania State University, University Park, PA, 2003.
[17] T. Poinsot, S. Lele, *J. Comput. Phys.* 101 (1992) 104–129.
[18] R.C. Swanson, E. Turkel, *J. Comput. Phys.* 101 (1992) 292–306.
[19] J.C. Oefelein, V. Yang, *J. Propul. Power* 14 (1998) 843–857.
[20] S. Apte, V. Yang, *Combust. Flame* 131 (2002) 110–131.
[21] Y.C. Chao, *AIAA J.* 26 (1988) 623–625.
[22] D. Peng, B. Merriman, S. Osher, H. Zhao, M. Kang, *J. Comput. Phys.* 155 (1999) 410–438.
[23] R.P. Fedkiw, G. Sapiro, C.W. Shu, *J. Comput. Phys.* 185 (2003) 309–341.